energies

MDPI

Article

Collaborative Control Strategy of Power Quality Based on Residual Capacity of Photovoltaic Inverter

Zekun Sun [1], Hao Liu [2], Yueming Ding [2], Haopeng Luo [1], Ting Liu [1] and Qinyue Tan [1,*]

[1] College of Water Resources and Architectural Engineering, Northwest A&F University, Xianyang 712100, China
[2] Rizhao Power Supply Company, State Grid Shandong Electric Power Company, Rizhao 276800, China
* Correspondence: qinyuetan@nwsuaf.edu.cn

Abstract: With the large-scale distributed PV connected to the grid, the random and intermittent nature of PV output, the non-linearity of the inverter, as well as the low daytime base-load and large-scale back feeding cause outstanding power quality problems such as overvoltage, three-phase unbalance, and high harmonic content at the end of the power supply system, which seriously affects the safe and stable operation of the grid and power efficiency. Based on the residual capacity of the inverter, this paper investigates a cooperative power quality control strategy that integrates active power filter, reactive power compensation, and inverter functions to achieve comprehensive power quality control and management without adding additional hardware equipment. The validation results show that the control strategy strongly improves the power quality, grid security, stability, and efficiency. This strategy indicates significant economic benefits.

Keywords: power quality; PV inverters; residual capacity; instantaneous power theory; cooperative control

check for updates

Citation: Sun, Z.; Liu, H.; Ding, Y.; Luo, H.; Liu, T.; Tan, Q. Collaborative Control Strategy of Power Quality Based on Residual Capacity of Photovoltaic Inverter. *Energies* **2022**, *15*, 8049. https://doi.org/10.3390/en15218049

Academic Editor: Abu-Siada Ahmed

Received: 26 September 2022
Accepted: 27 October 2022
Published: 29 October 2022

Publisher's Note: MDPI stays neutral with regard to jurisdictional claims in published maps and institutional affiliations.

Copyright: © 2022 by the authors. Licensee MDPI, Basel, Switzerland. This article is an open access article distributed under the terms and conditions of the Creative Commons Attribution (CC BY) license (https://creativecommons.org/licenses/by/4.0/).

1. Introduction

With the rapid development of wind, light, and other new energy generation, the distribution network presents a development trend of high-proportion distributed generation. A total of 54.88 million kW was added in 2021, and by the end of 2021 China's installed photovoltaic capacity had reached 310 million kW [1].

Large-scale distributed photovoltaic access to the grid, coupled with the randomness and intermittency of photovoltaic output, non-linear inverter, as well as the low daytime base load and large-scale back feeding cause outstanding power quality problems, such as overvoltage, three-phase unbalance, and high harmonic content at the end of the supply and consumption system [2,3]. Incidents of system failure and equipment damage caused by photovoltaic grid connection occurs occasionally. The safety, stability, and power quality problems caused by photovoltaic power generation are also becoming more and more prominent, and there are more and more equipment damage accidents caused by harmonic and overvoltage [4–7]. Therefore, there is urgent need to explore an effective governance strategy to alleviate the serious voltage problem in distribution networks. In addition, precision digital power supply and load equipment, are more sensitive to voltage, and higher voltage power quality is required.

DC/AC conversion is the core link of photovoltaic power generation, and its control strategy determines the performance of the inverter [8,9]. The two-stage photovoltaic system is controlled separately in the front and rear stages, which is simpler than the single-stage system and is widely used in distributed photovoltaic power generation [10–13]. Due to the influence of even harmonics on the DC side, the two-stage grid-connected inverter will produce the second low-frequency ripple component on the DC bus capacitor [14–16]. Excessive ripple voltage will lead to output voltage distortion, and excessive ripple current will make the bus capacitor produce heat and shorten its life [16–18]. At the same time,

the second harmonic affects the maximum power point tracking (MPPT) control, which reduces the photoelectric conversion efficiency of photovoltaic panels.

The distributed PV grid-connected inverter has the same main circuit topology as the active filter (APF) and the static reactive power generator (SVG), so the grid-connected inverter can be used for both harmonic control and reactive power compensation. By using a multi-function inverter (MFINV) with harmonic control functions as the grid connection interface for distributed power supplies, the residual capacity can be used to assist in harmonic and reactive power control [19–22]. Control strategies for simultaneous harmonic, reactive power, and negative sequence compensation using multifunctional inverters were investigated for power quality problems such as harmonics, voltage deviation, and three-phase unbalance [19,20]. In the literature [21], control strategies were also designed for different DG output and power demand conditions to ensure grid connection and active filtering under different supply and demand conditions. A direct control strategy of inverter impedance to realize harmonic sharing was proposed [22].

Many studies have been conducted on the current tracking control technology of multifunctional PV grid-connected inverters and grid-connected system control strategies [23]. The unified control of active filters and PV grid connection has been investigated [24–26], focusing on algorithms for the synthesis of active and harmonic compensation currents in PV grid connection. In, the literature [27,28], the control of SVG with PV grid-connected power generation was unified, using the residual capacity of PV inverters for reactive power compensation and suppressing grid voltage fluctuations. All the above involve the residual capacity of PV power generation with active grid connection for power quality management, but the authors did not consider whether PV power generation could be generated at full power under harmonic and overvoltage conditions.

Based on the three-phase non-isolated photovoltaic grid-connected two-stage system, this paper examines the influence of AC side harmonics on the maximum power point of photovoltaic. On this basis, the improved conductance increment method (INC algorithm) is used to replace the traditional MPPT algorithm to reduce the influence of grid harmonics on MPPT and stabilize the voltage of the BOOST circuit. Doing so ensures that the multifunctional inverter first meets the maximum power of the PV to the grid, improves the utilization rate of the inverter, and performs harmonic and reactive power management based on the residual capacity of the inverter. This provides a theoretical basis for improving the tracking capability of the maximum power point and power quality management for the operation of two-level PV grid-connected systems.

2. Influence of Harmonics on Photovoltaic Power Generation System

2.1. Influence of Harmonics on Grid-Connected System

For this study, an LCL filter was chosen as the photovoltaic grid-connected filter [29–31], which has a simple structure, easy control, and better filtering performance and high-frequency harmonic attenuation. The LCL-type filter topology is shown in Figure 1. The block diagram of the LCL mathematical control model is shown in Figure 2.

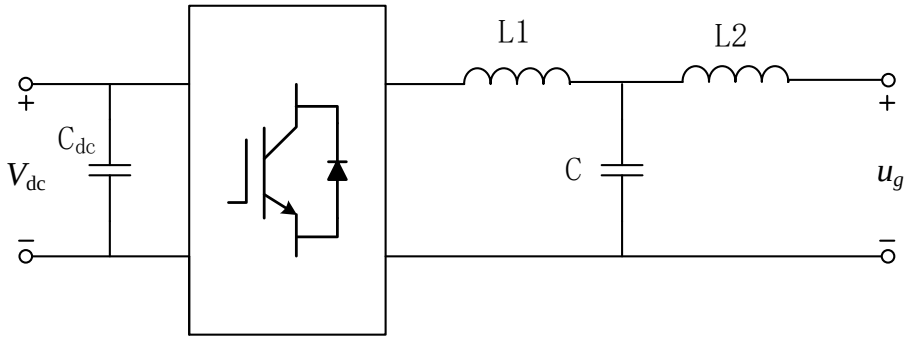


Figure 1. The LCL-type filter topology.

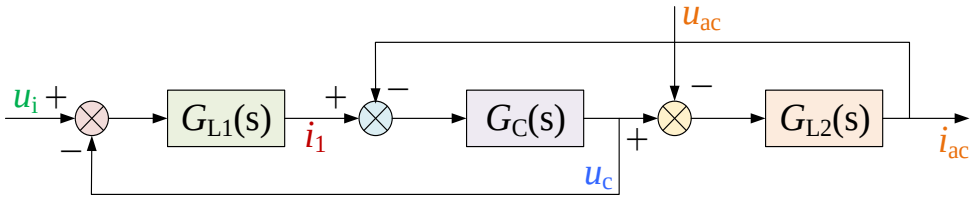


Figure 2. LCL mathematical control model block diagram.

The inverter output voltage is u_i, while u_{ac} and i_{ac} are photovoltaic grid voltage and current, respectively. The transfer function between the input voltage of the filter and the grid-connected current satisfies Formula (1), where L_1, L_2, and C are the inductance and capacitance values of the LCL filter marked in Figure 2.

$$\frac{I_{ac}(s)}{U_i(s)} = \frac{1}{L_1 L_2 C^3 + (L_1 + L_2)s} \tag{1}$$

Thus, the resonant frequency expression of the filter satisfies the Formula (2).

$$f_{res} = \frac{1}{2\pi}\sqrt{\frac{L_1 + L_2}{L_1 L_2 C}} \tag{2}$$

The distortion of the grid current due to the injection of harmonics can lead to parallel resonance in the LCL circuit, which can lead to large currents flowing in the inductive and capacitive components, thus burning out the electrical equipment. The additional circuit losses due to harmonics are also increased due to the skin effect of the wires.

2.2. Influence of Secondary Ripple on MPPT

The two-stage photovoltaic topology is shown in Figure 3.

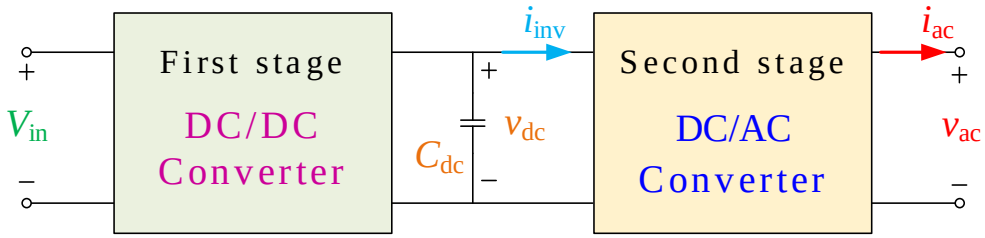


Figure 3. Topological structure of two-stage grid-connected system.

A two-stage photovoltaic system is directly connected to the grid, and the instantaneous values of grid voltage and current meet Formulas (3) and (4), respectively. Where V_{ac}, I_{ac} are the RMS values of voltage and current, and θ is the phase angle of grid voltage and current. It can be derived that the inverter output power satisfies Equation (5).

$$v_{ac}(t) = \sqrt{2}V_{ac}sin\omega t \tag{3}$$

$$i_{ac}(t) = \sqrt{2}I_{ac}sin(\omega t - \theta) \tag{4}$$

$$p_0(t) = v_{ac}(t)i_{ac}(t) = V_{ac}I_{ac}[2sin\omega t \cdot sin(\omega t - \theta)] = V_{ac}I_{ac}[cos\theta - cos(2\omega t - \theta)] \tag{5}$$

In Equation (6), ignoring the power loss, is the reactive power in the inverter filter inductor and filter capacitor of the post-stage DC/AC converter; that is, the input power and output power of the post-stage meet.

$$p_{inv}(t) = p_0(t) \tag{6}$$

The average value of the intermediate bus voltage is V_{dc}, and the current $i_{inv}(t)$ transmitted by the intermediate bus capacitor to the back-stage converter satisfies Equation (7). The composition of $i_{inv}(t)$ of the back-stage inverter includes the DC current component and the double grid frequency ripple component, where the DC component represents the active power of the back-stage inverter. Traffic isolation is the basic characteristic of a capacitor, so bus capacitor C_{dc} provides twice the power frequency ripple component in the instantaneous input current of the inverter. The instantaneous input of capacitor current of an intermediate bus is $i_{dc}(t)$ satisfying (8).

$$i_{inv}(t) = \frac{p_{inv}(t)}{V_{dc}} = \frac{V_{ac}I_{ac}}{V_{dc}}cos\theta - \frac{V_{ac}I_{ac}}{V_{dc}}cos(2\omega t - \theta) \tag{7}$$

$$i_{dc}(t) = \frac{V_{ac}I_{ac}}{V_{dc}}cos(2\omega t - \theta) \tag{8}$$

From Equation (8), the voltage ripple of the intermediate bus capacitor satisfies Equation (9), and thus the voltage u_{dc} of the intermediate bus capacitor satisfies Equation (10).

$$\Delta u_{dc} = \frac{1}{C_{dc}}\int \frac{V_{ac}I_{ac}}{V_{dc}}cos(2\omega t - \theta)dt = \frac{V_{ac}I_{ac}}{2\omega C_{dc}V_{dc}}sin(2\omega t - \theta) = \frac{P_0}{2\omega C_{dc}V_{dc}}sin(2\omega t - \theta) \tag{9}$$

$$u_{dc} = V_{dc} + \Delta u_{dc} \tag{10}$$

Without considering the front and rear converter and line loss, the second harmonic current is provided by the front DC/DC converter and the intermediate bus capacitor. Therefore, the intermediate bus voltage oscillates near the target value. Because MPPT tracking requires a duty cycle to modulate the PWM waveform to drive the DC/DC converter when the intermediate bus voltage of the BOOST circuit is about to affect the maximum power point oscillates, the output power of photovoltaic cells oscillates near the maximum power point, resulting in solar cells that cannot achieve MPPT tracking well.

MPPT tracking is based on any disturbance technique: the MPPT controller for the perturbation observation method and the conductance increment method may cause a miscalculation when the PV is tracking the maximum power point, i.e., and make the MPPT algorithm crash; the active output of the PV cell is even lower and the efficiency of the system may be severely lost, which is not conducive to grid connection. The P-V and I-V curves of PV output under secondary ripple are shown in Figure 4.

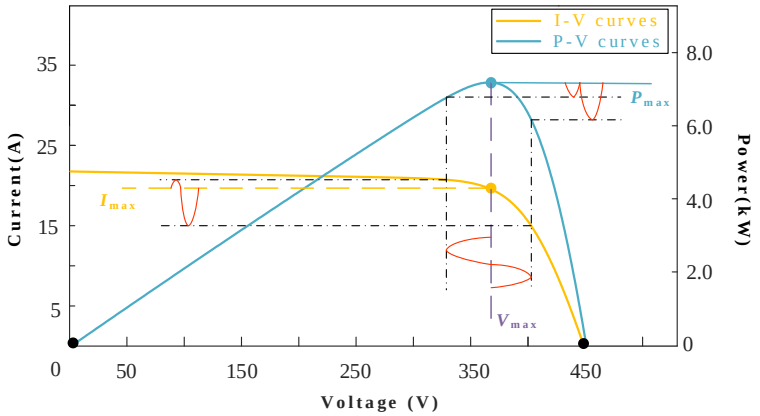


Figure 4. P-V and I-V curves of photovoltaic output under secondary ripple.

2.3. The Improvement of MPPT Algorithm

The traditional incremental conductance method often uses a fixed step size, which needs to be weighed in the dynamic response and steady-state oscillation. In order to meet the dynamic response and steady-state output at the same time, the traditional algorithm

with a fixed step size adopts a compromised duty cycle variation. However, at this time, the environmental conditions change rapidly or the second harmonic is large, which will lead to the failure of the algorithm and cannot meet the photovoltaic grid-connected conditions.

In this paper, the variable step-size INC method is proposed, and the variable step-size is automatically adjusted according to the inherent characteristics of the photovoltaic array. If the operating point is far from the maximum power point, the step-size increases to ensure rapid tracking. If the operating point is near the maximum power point, the step-size is smaller, the oscillation is reduced, and the efficiency is improved. The variable step-size method has better dynamic performance, can quickly track the maximum power point, and is not easily affected by external conditions and secondary ripple. Variable step incremental conductance method combined with duty cycle is used to control the maximum power point tracking of photovoltaic. The variable step INC process is shown in Figure 5.

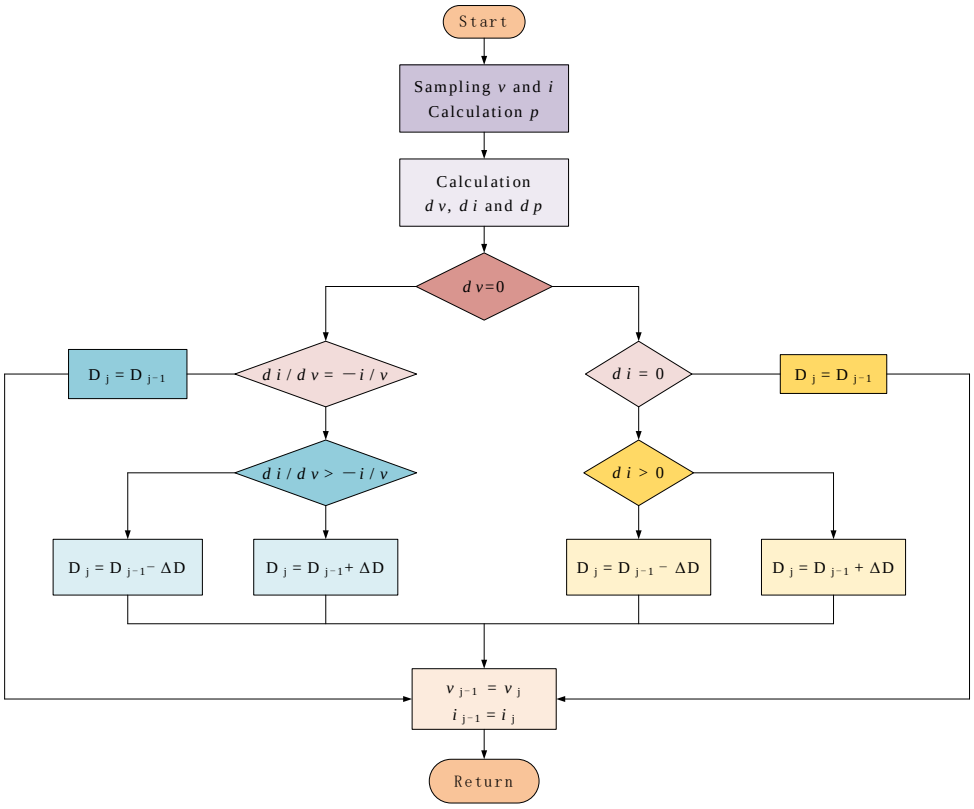


Figure 5. Variable step INC flow chart.

In Figure 5, the duty cycle is D, and the change of each duty cycle is Δ D = K × step, where K = n × abs (dp/dv), n is a constant, n = 0.0002. The value of step is shown in Table 1:

Table 1. Value table of step.

Constraint Condition		Values
$dv = 0$	$di = 0$	step = 0
	$di > 0$	step = 1
	$di < 0$	step = −1
$dv \neq 0$	$di/dv = -v_2/v_1$	step = 0
	$di/dv > -v_2/v_1$	step = −1
	$di/dv < -v_2/v_1$	step = 1

This method ensures that the PV always outputs power near the maximum power point and can satisfy the economics of the inverter. The power quality control strategy is based on the maximum power output.

3. Multi-Functional Photovoltaic Grid-Connected Inverter

3.1. Active Filter

An active power filter (APF) is widely used in power systems. As shown in Figure 6, in the working process of the active power filter, it is necessary to first collect the harmonic current signal from the load side to improve the power quality. After the operation of the instruction current operation circuit, the synthesized instruction signal is sent to the current tracking control circuit. Then, the current tracking control circuit controls the drive circuit, and the drive circuit controls the gate opening of the main circuit. The PWM converter is used to send out the waveform; that is, reverse phase to the harmonic current and output to the load side to be compensated, thus the purpose of harmonic elimination is achieved.

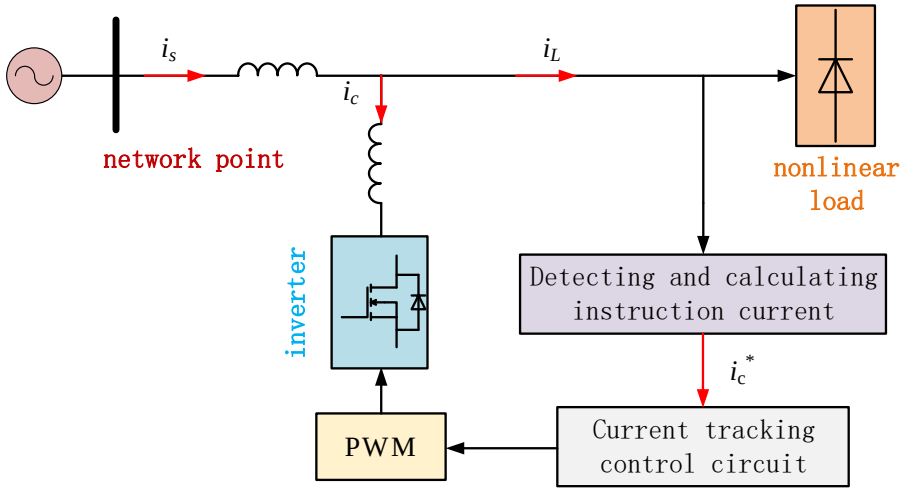


Figure 6. Basic principle diagram of active filter.

The basic working principle expression of the active power filter satisfies Equation (11).

$$i_s = i_L + i_c = (i_{Lf} + i_{Lh}) + (-i_{Lh}) = i_{Lf} \tag{11}$$

where i_s is the supply current; i_L is the load current to be compensated; i_c is the compensation current, which is the inverter output current; i_{Lf} is the fundamental component of the load current; i_{Lh} is the harmonic component of the load current.

3.2. Improved Harmonic Current Detection Method

Using the instantaneous reactive power theory, the phase-locked loop to obtain the sine cosine signal of the same phase of the a-phase voltage is set. According to the above definition of the load current coordinate transformation, by Clark transformation and Park transformation, i_p, i_q are extracted from i_a, i_b, i_c; after LPF, the DC components $\overline{i_p}$, $\overline{i_q}$ are obtained and then calculated from the fundamental components i_{af}, i_{bf}, i_{cf}, and it can further be obtained from the harmonic components i_{ah}, i_{bh}, i_{ch}.

The analysis and simulation are carried out in the case of no distortion of the grid voltage and the three-phase symmetry, then the three-phase voltage e satisfies Equation (12). The load-side currents containing harmonics satisfy Equation (13). The three-phase harmonic currents i_a, i_b, i_c satisfy Equation (14) after a coordinate transformation, where C_{32} satisfies Equation (15).

$$\begin{bmatrix} e_a \\ e_b \\ e_c \end{bmatrix} = \begin{bmatrix} \sqrt{2}E_1 \sin \omega t \\ \sqrt{2}E_1 \sin(\omega t - 2\pi/3) \\ \sqrt{2}E_1 \sin(\omega t + 2\pi/3) \end{bmatrix} \tag{12}$$

$$\begin{bmatrix} i_a \\ i_b \\ i_c \end{bmatrix} = \begin{bmatrix} \sum_{n=1}^{\infty} \sqrt{2} I_n \sin(n\omega t + \varphi_n) \\ \sum_{n=1}^{\infty} \sqrt{2} I_n \sin[n(\omega t - 2\pi/3) + \varphi_n] \\ \sum_{n=1}^{\infty} \sqrt{2} I_n \sin[n(\omega t + 2\pi/3) + \varphi_n] \end{bmatrix} \tag{13}$$

$$\begin{bmatrix} i_p \\ i_q \end{bmatrix} = \begin{bmatrix} \sin\omega t & -\cos\omega t \\ -\cos\omega t & -\sin\omega t \end{bmatrix} \cdot C_{32} \begin{bmatrix} i_a \\ i_b \\ i_c \end{bmatrix} = \begin{bmatrix} \sin\omega t & -\cos\omega t \\ -\cos\omega t & -\sin\omega t \end{bmatrix} \cdot \begin{bmatrix} i_\alpha \\ i_\beta \end{bmatrix} \tag{14}$$

$$C_{32} = \begin{bmatrix} 1 & -1/2 & -1/2 \\ 0 & \sqrt{3}/2 & -\sqrt{3}/2 \end{bmatrix} \tag{15}$$

By combining Equations (13) and (14), it can be verified that i_p and i_q satisfy Equation (16) and its DC component satisfies Equation (17) after being filtered by the low-pass filter. This results in the fundamental and harmonic currents obtained after the filtering of the load current, satisfying Equations (18) and (19), respectively.

$$\begin{bmatrix} i_p \\ i_q \end{bmatrix} = \sqrt{3} \begin{bmatrix} \sum_{n=1}^{\infty} I_n \cos[(1 \mp n)\omega t \mp \varphi_n] \\ \sum_{n=1}^{\infty} \pm I_n \sin[(1 - n)\omega t - \varphi_n \end{bmatrix} \tag{16}$$

$$\begin{bmatrix} \overline{i_p} \\ \overline{i_q} \end{bmatrix} = \sqrt{3} \begin{bmatrix} I_1 \cos(-\varphi_1) \\ I_1 \sin(-\varphi_1) \end{bmatrix} \tag{17}$$

$$\begin{bmatrix} i_{af} \\ i_{bf} \\ i_{cf} \end{bmatrix} = C_{23} \cdot \begin{bmatrix} \sin\omega t & -\cos\omega t \\ -\cos\omega t & -\sin\omega t \end{bmatrix} \cdot \begin{bmatrix} \overline{i_p} \\ \overline{i_q} \end{bmatrix} = \begin{bmatrix} \sqrt{2} I_1 \sin(\omega t + \varphi_1) \\ \sqrt{2} I_1 \sin(\omega t - 2\pi/3 + \varphi_1) \\ \sqrt{2} I_1 \sin(\omega t + 2\pi/3 + \varphi_1) \end{bmatrix} \tag{18}$$

$$\begin{bmatrix} i_{ah} \\ i_{bh} \\ i_{ch} \end{bmatrix} = \begin{bmatrix} i_a \\ i_b \\ i_c \end{bmatrix} - \begin{bmatrix} i_{af} \\ i_{bf} \\ i_{cf} \end{bmatrix} \tag{19}$$

When it is used for the active filter and reactive power compensation, harmonic and reactive current need to be detected at the same time. At this time, the detection of the q channel is disconnected; that is, the expression of the sum of harmonic and reactive current satisfies (20). In order to ensure that the output power of photovoltaic cells remains at the maximum power point, it is necessary to stabilize the DC bus voltage so as to ensure the active output of photovoltaic cells.

$$\begin{bmatrix} i_{ah} + i_{aq} \\ i_{bh} + i_{bq} \\ i_{ch} + i_{cq} \end{bmatrix} = \begin{bmatrix} i_a \\ i_b \\ i_c \end{bmatrix} - C_{23} \cdot \begin{bmatrix} \sin\omega t & -\cos\omega t \\ -\cos\omega t & -\sin\omega t \end{bmatrix} \cdot \begin{bmatrix} \overline{i_p} \\ 0 \end{bmatrix} \tag{20}$$

Then, i_p, i_q are changed into DC components $\overline{i_p}$, $\overline{i_q}$ through the LPF. LPF generally uses the second-order Butterworth filter and cut-off frequency is in 15~40 Hz. This paper selected 20 Hz for analysis and comparison. Although the second-order filter has good filtering performance, it also has a large delay. Therefore, the average current method is used for the input of the low-pass filter on this basis. The average current method process is shown in Figure 7.

The following is a simulation analysis of the two schemes. Based on the instantaneous power theory, the instantaneous power theory harmonic detection method is used. The simulation uses an ideal power supply with no distortion of 220 V as the parallel point, and the simulation starts with a non-linear load connected at 0 s, and the resistance of the non-linear load is reduced to half of the original value at 0.15 s. Simulation results are shown in Figure 8.

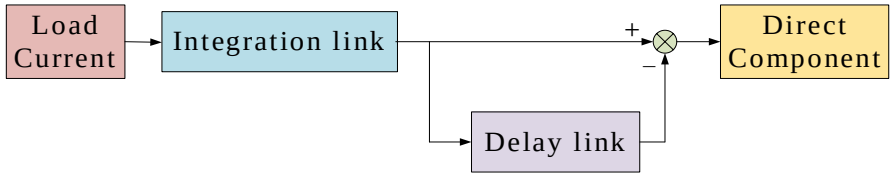


Figure 7. Average current filtering process.

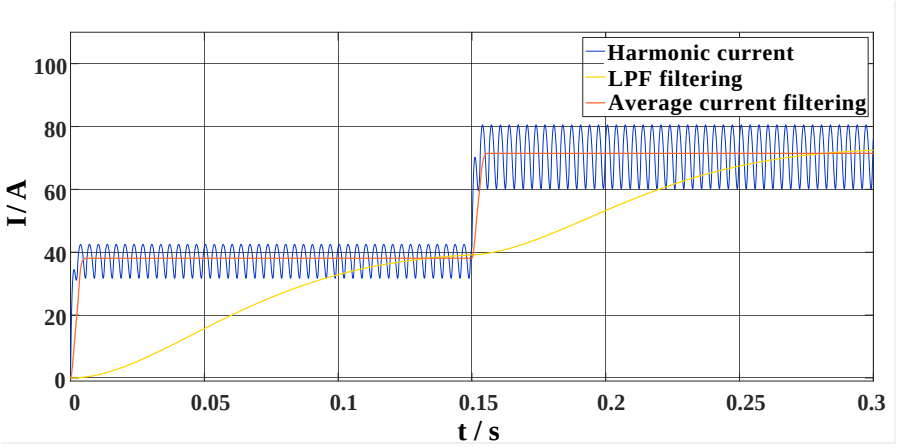


Figure 8. Comparison of LPF filtering and average current filtering schemes.

As shown in Figure 8, although the second-order Butterworth filter can achieve a good filtering effect, its response is slow and cannot be filtered in time, so it is not as proficient at carrying out harmonic detection and real-time harmonic compensation. The average current method can filter quickly and reduce the filtering delay to T/6 period so as to conduct harmonic detection faster and achieve fast harmonic compensation ability. When the non-linear load changes 0.15 s, the harmonic current i_p changes rapidly, and the average current method can also track and filter quickly. Therefore, the average current method is used to replace the traditional second-order Butterworth filter.

3.3. Current Synthesis Instruction

For distributed PV grid-connected inverters, three operating states are designed for the purpose of power quality management based on the remaining capacity of the inverter. In the first state, the entire capacity is used for the DC/AC inverter function for grid-connected power generation; in the second state, the DC/AC inverter for grid-connected power generation is prioritized, followed by the remaining capacity for power quality management; in the third state, the entire capacity is used for power quality management in the absence of light. In addition, when the remaining capacity is not sufficient for power quality management, additional filtering devices such as APF can be considered for further compensation.

First, the output current of the photovoltaic array is collected, and the output voltage reference value U_{PV}^{*} is obtained by MPPT maximum power tracking method. Compared with the actual output voltage U_{PV} of photovoltaic array, the active command current i_p of photovoltaic array output is obtained by PI control. Then, the load-side current is detected. A normal value ε is set, and the detected harmonic current A normal value ε is compared. Through further calculation, i_c is obtained as the current that needs compensation in the system.

The output power of the inverter satisfies Equation (5). In this paper, the inverter AC side voltage is the line voltage of the grid, which is stable at 380 V, so the inverter output power changes are reflected in the inverter output current changes. Therefore, the residual capacity of the inverter can be expressed in terms of the magnitude of the residual current. The rated current of the inverter satisfies (21), where i_n is the rated current of the inverter,

i_p is the active command current of the photovoltaic grid, and i_{AMP} is the residual capacity of the inverter.

$$i_n = i_p + i_{AMP} \tag{21}$$

Considering the limited installed capacity and compensation capacity of the inverter, this paper only uses the residual capacity of the grid-connected inverter to compensate for the harmonics and reactive currents at the grid connection point of the microgrid, so the solution method firstly satisfies the output of active power of the PV. In order to ensure the safety and economy of the photovoltaic grid-connection, harmonic control in this paper is engaged prior to reactive power compensation. The flow diagram of the inverter for grid-connected PV and power quality management is shown in Figure 9. Where i is the actual inverter output current; i_h, i_q are the detected and calculated harmonic currents and reactive currents to be compensated, respectively; K_1, K_2, and K_3 are three parameters from 0 to 1, which make the inverter output current less than the rated current.

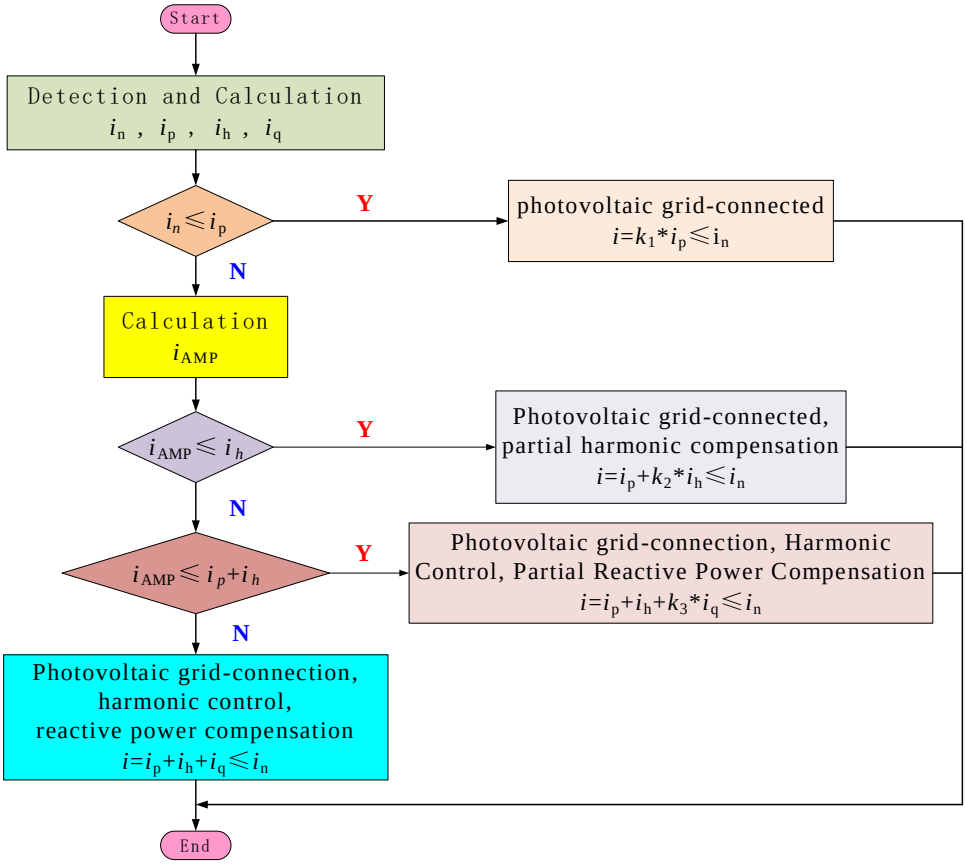


Figure 9. The flow diagram of power quality control for photovoltaic grid-connected.

In order to solve the leakage current problem of the two-stage photovoltaic grid-connected and power quality control system, the intermediate DC bus adopts two equal capacitors, and the grid-connected end and the midpoint of the DC bus are grounded. The improved two-stage system diagram is shown in Figure 10.

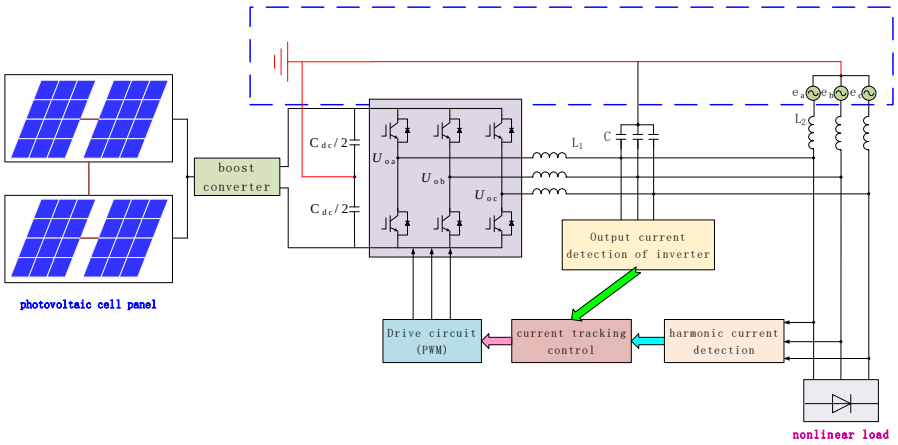


Figure 10. Improved two-stage system block diagram.

4. Simulation Analysis

In order to verify the theoretical analysis, a simulation model is built using Matlab/Simulink for qualitative and quantitative analysis. The system is structured using the diagram above, where the main parameters are shown in Table 2.

Table 2. Main parameters of improved two-stage system.

Structure Name	Units	Value	Structure Name	Units	Value
PV MPPT Current	A	20.0	Filter Inductance L_1	mH	1.5
PV MPPT Voltage	V	364.0	Filter Capacitance C	μF	3000.0
DC Bus Capacitor C_{dc}	μF	2 × 800.0	Filter Inductance L_2	mH	0.6

4.1. Simulation of Harmonic Influence on DC Side

Before 0.5 s, when the grid uses an ideal supply at infinity, no harmonic currents are injected and the PV is only grid-connected; after 0.5 s, the grid is contaminated by harmonics and the simulation is analyzed on this basis. The DC bus voltage simulation diagram is shown in Figure 11.

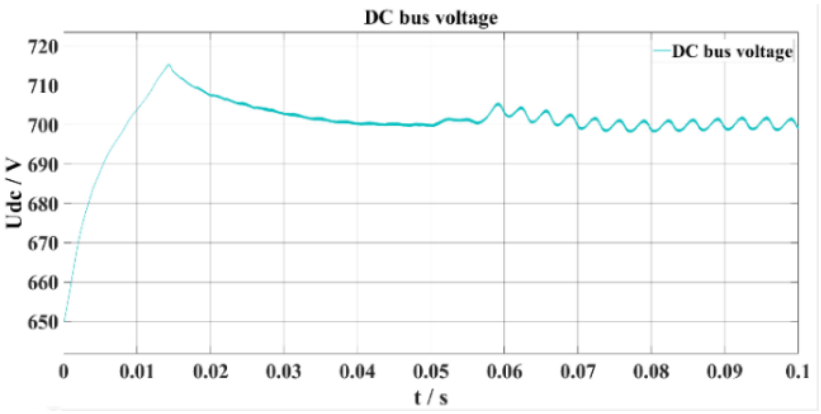


Figure 11. DC bus voltage simulation diagram.

The intermediate DC bus voltage can be stabilized at 700 V before 0.05 s, due to the injection of harmonic current at 0.05 s, which leads to distortion of the grid current and thus affects the DC bus voltage, making it oscillate back and forth around 700 V, which does not allow the PV to operate at full power and affects the active current output of the PV to the grid. Harmonic compensation is therefore inevitable.

Under the influence of the secondary ripple, the PV maximum power point tracking in the premise of the variable step conductance increment method, PV ensures the output of active power at the maximum power point; 0.05 s grid current injection harmonics, PV maximum power tracking as shown in Figure 12.

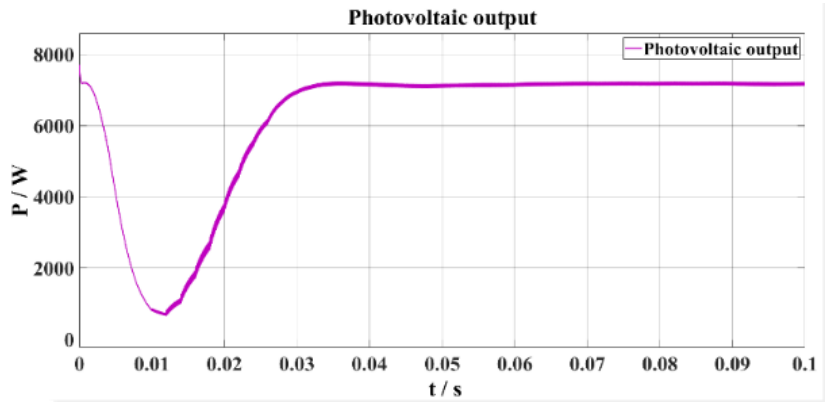


Figure 12. Maximum power point tracking.

According to Figure 12, with the variable step INC algorithm, the PV output power is stable at around 7.2 kW, which can continuously track the maximum output power better, with minimal influence from harmonics and external environment, and can achieve accurate MPPT tracking, which can better ensure the BOOST circuit to step up to the 700 V target value.

4.2. Simulation and Test Verify of Power Control Based on Residual Capacity of Inverter

4.2.1. Simulation of Power Control Based on Residual Capacity of Inverter

This paper selected the inverter capacity of 10 kW, considering the photovoltaic inverter has both source filtering and reactive power compensation function, inverter switching frequency is 10 kHz, in order to simulate the actual inverter dynamic performance, inverter Rs (Ohms) is set to inf, Cs (F) is set to 0. The maximum output power of photovoltaic cells is 7280 W, and photovoltaic grid-connected generation is connected to the grid at the maximum power point. When DC-DC and DC-AC circuits have certain losses, assuming that the active power of photovoltaic grid-connected is the 7000 W, the remaining capacity of the inverter is 30%, which can be used for active filtering and reactive power compensation.

When photovoltaic grid-connection and active filtering are carried out, referred to as Mode 1 in this paper, and the simulation results of grid-connected current are shown in Figure 13. Harmonic analysis and power factor are shown in Figures 14 and 15, respectively.

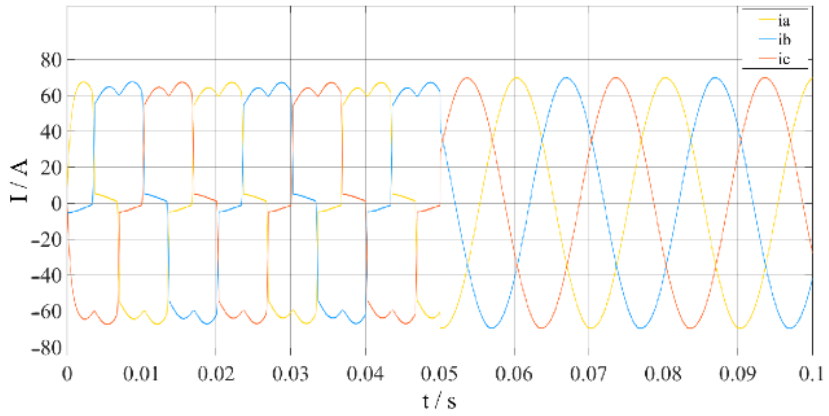
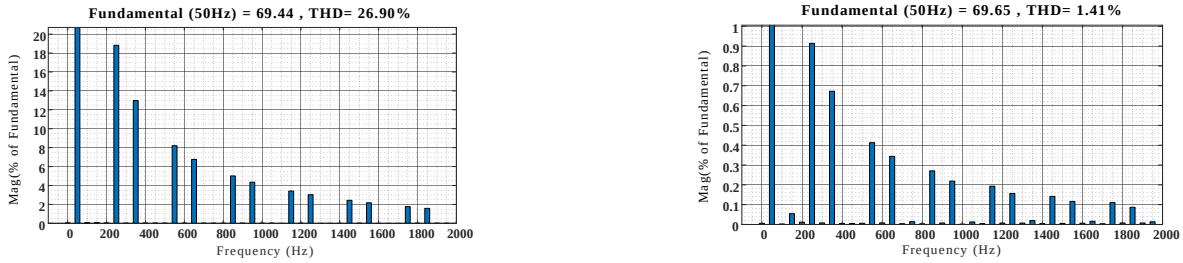


Figure 13. Mode 1 grid current diagram.



(**a**) (**b**)

Figure 14. Mode 1 harmonic analysis diagram. (**a**) Harmonic analysis diagram before harmonic treatment. (**b**) Harmonic analysis diagram after harmonic treatment.

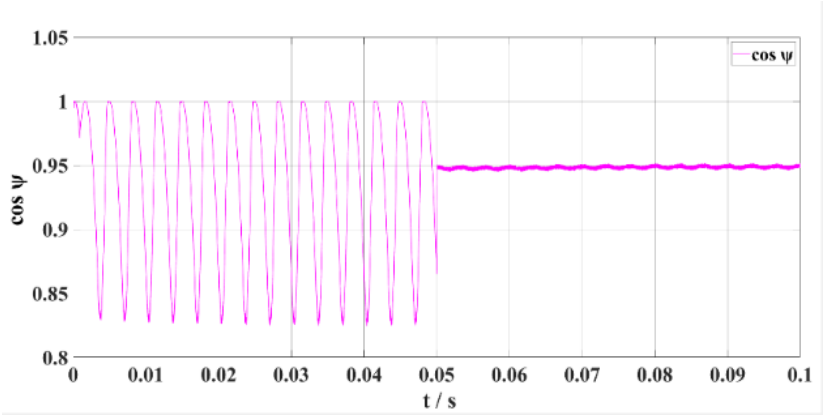


Figure 15. Mode 1 grid-connected power factor.

A value of 0.05 s is chosen to start harmonic compensation. According to Figure 14a,b, the harmonic amount before treatment is 26.90%, and the harmonic amount after treatment is reduced to 1.41%, which has good filtering ability and meets the requirements of grid connection. Figure 14 shows that the power factor of the grid without reactive power compensation is about 0.95, and the power factor is low.

When grid-connected PV, active filtering, and reactive power compensation are carried out simultaneously, referred to as Mode 2 in this paper, the grid-connected current simulation results are shown in Figure 16. Harmonic analysis and power factor are shown in Figures 17 and 18, respectively.

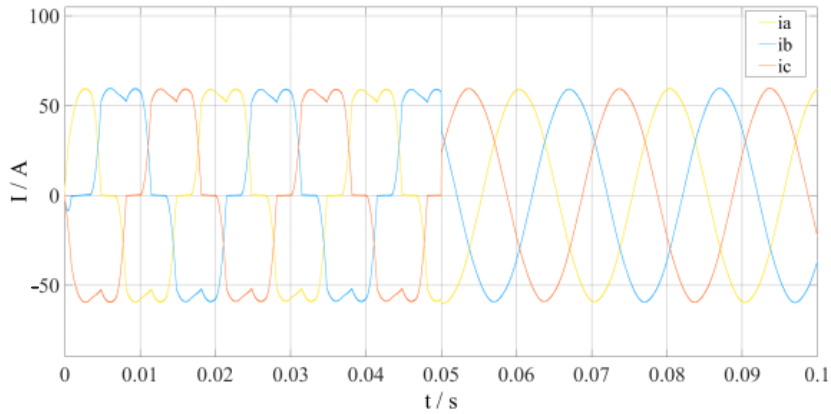


Figure 16. Mode 2 grid current diagram.



Figure 17. Mode 2 harmonic analysis diagram. (**a**) Harmonic analysis diagram before harmonic treatment. (**b**) Harmonic analysis diagram after harmonic treatment.

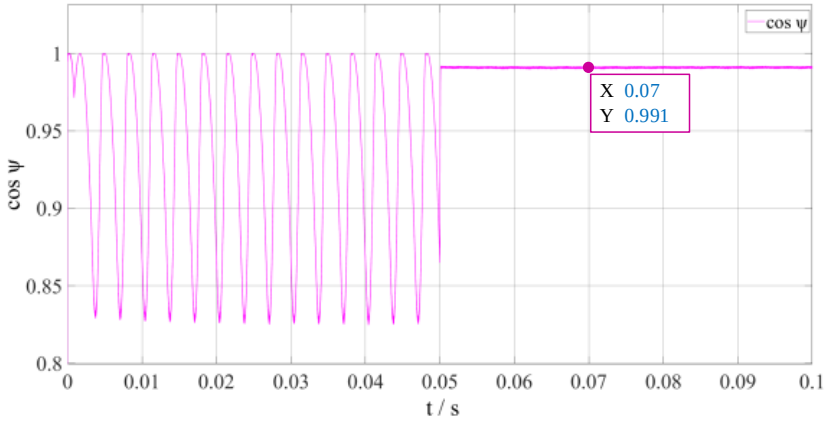


Figure 18. Mode 2 grid-connected power factor.

Harmonic and reactive power compensation starts at 0.05 s. According to the two diagrams in Figure 17a,b, it is seen that the amount of harmonics after the treatment is 2.70% and the power factor is around 0.99, which has good filtering capacity and reactive power compensation capacity to meet the grid connection requirements.

Due to the remaining capacity limitation, the hybrid PV grid-connected, harmonic and reactive power compensation mode has a slightly lower harmonic compensation capacity than the hybrid PV grid-connected and harmonic compensation mode, but it can improve the power factor and grid-connection while reducing harmonic and reactive power hazards.

Combining Figures 16 and 18, the number of harmonics contained in the currents can all meet the requirements for grid connection, and this active filtering and reactive power compensation can better meet the higher standards. The capacity of active filtering based on the remaining capacity of the inverter is limited, and there is greater ability to manage harmonic currents and reactive shocks when they are not very large.

4.2.2. Test Verify of Power Quality Control Based on Residual Capacity of Inverter

The multifunctional inverter with a capacity of 10 kW is used in this paper for preliminary performance index test. The photovoltaic part is replaced by a DC power supply and the inverter also performs grid connection and power management functions. The parameters of the experimental part are shown in Table 3. The experimental scene is shown in Figure 19.

Table 3. The Experimental parameters.

Parameters Name	Units	Value	Parameters Name	Units	Value
DC Voltage	V	550~750	Inverter Efficiency	%	≥95
DC Current	A	0~18.2	IGBT (U_N, I_N)	V, A	1200, 225
DC Voltage Precision	%	≤1	Filter Inductance L_1	mH	2.4
Switching Frequency	kHz	10	Filter Capacitance C	μF	3.3
Control Response Time	ms	≤100	Filter Inductance L_2	mH	1.2

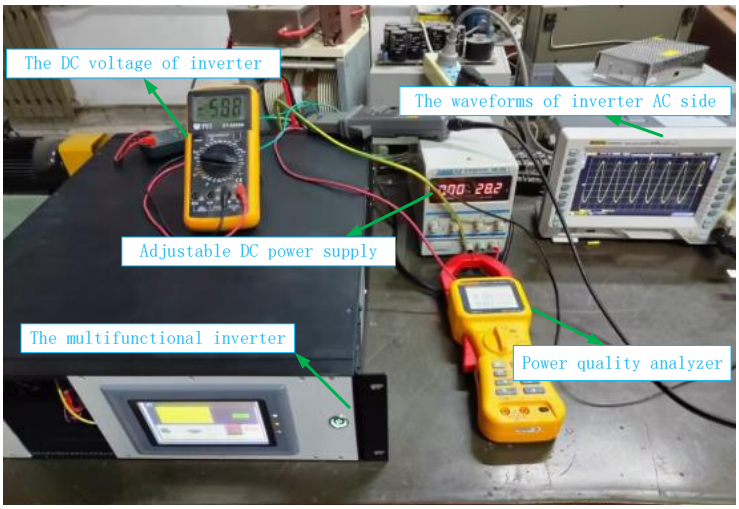


Figure 19. The experimental scene.

In the experimental part, the test shows that the voltage fluctuation of the AC side is within 5%, the power factor is around 0.96, and the harmonic distortion rate total harmonic distortion (THD) is 2.96%, which are consistent with simulation results.

5. Conclusions

Based on the PV inverter residual capacity and instantaneous power theory, this paper uses the PV grid-connected active current to synthesize the command current and improve the filtering method in harmonic current detection, taking the three-phase two-stage PV grid-connected system as the research object, using an improved two-stage PV grid-connected system and MPPT algorithm to meet the PV grid-connected maximum power condition operation while performing active filtering and reactive power compensation.

(1) The presence of LPF in the traditional harmonic detection method leads to slower system response. An improved filter detection method is proposed, using a current averaging module instead of a low-pass filter, with a system response speed of only 1/6 of the current period, substantially improving the response speed of harmonic and reactive current detection.

(2) The improved two-stage PV grid-connected system can reduce the leakage current between the two stages while using the variable step INC algorithm for MPPT tracking to ensure the maximum output power of the PV cell, and use the residual capacity of the inverter for harmonic management and reactive power compensation. The operation results show that the new MPPT algorithm can effectively reduce the impact of DC bus voltage ripple on MPPT tracking and ensure the PV MPPT tracking speed. The power quality control is based on MPPT tracking. Simulation analysis shows that the MPPT algorithm of the front stage BOOST circuit can guarantee the maximum power output from the PV and the back stage can be effectively controlled according to the residual capacity.

(3) Analysis and simulation results show that the collaborative power quality control strategy based on the residual capacity utilization of PV inverters can perform active filtering (APF) and reactive power compensation (SVG) quickly and accurately, effectively

reducing harmonic content and voltage fluctuations, increasing the power factor to 0.99, reducing the current distortion rate to 2.71%, and significantly improving the harmonic content of the three-phase two-stage PV grid-connected system in terms of safety, stability, and economy. The preliminary experimental results show that the performance index of the multifunctional inverter is consistent with the simulation and analysis.

Author Contributions: Conceptualization, Z.S. and Q.T.; methodology, Q.T.; software, Z.S.; validation, Y.D., H.L. (Haopeng Luo) and H.L. (Hao Liu); formal analysis, Z.S.; investigation, Y.D.; resources, Y.D. and H.L. (Hao Liu); data curation, T.L.; writing—original draft preparation, Z.S.; writing—review and editing, H.L. (Haopeng Luo) and T.L.; visualization, Z.S.; supervision, Q.T.; project administration, Y.D.; funding acquisition, H.L. (Hao Liu). All authors have read and agreed to the published version of the manuscript.

Funding: This research was funded by State Grid Corporation Headquarters Science and Technology Project (5400-202216167A-1-1-ZN); Project Supported by National Nature Science Foundation of China (51577157).

Data Availability Statement: Not applicable.

Conflicts of Interest: The authors declare no conflict of interest.

References

1. State Energy Agency Online Press Conference Transcript in the First Quarter of 2022. Available online: http://www.nea.gov.cn/202201/28/c_1310445390.htm (accessed on 28 January 2022).
2. Liu, C. Consideration of distributed photovoltaic power generation access to rural distribution network. *Rural. Electician* **2022**, *30*, 31. [CrossRef]
3. Giri, A.K.; Arya, S.R.; Maurya, R.; Chittibabu, B. Control of VSC for enhancement of power quality in off-grid distributed power generation. *IET Renew. Power Gener.* **2020**, *14*, 771–778. [CrossRef]
4. Diaz-Araujo, M.; Medina-Rios, A.; Madrigal-Martinez, M.; Cleary-Balderas, L.A. Analysis of Grid-Connected Photovoltaic Generation Systems in the Harmonic Domain. *Energies* **2019**, *12*, 4785. [CrossRef]
5. Wang, R.; Yang, K.; Xie, X.; Shen, D.; He, L.; Chen, R.; Jing, H. The impact of photovoltaic power generation access on the voltage quality of distribution network. *Electr. Eng. Mater.* **2021**, *13*, 42–44. [CrossRef]
6. Wang, J.; Liu, Z.; Song, Q.; Xu, J. Analysis of distributed photovoltaic grid harmonic impact and governance. *Sci. Technol. Vis.* **2018**, 131–132. [CrossRef]
7. Deepamangai, P.; Manoharan, P.S. Detection and estimation of grid-connected issues in quasi-Z-source inverter based photovoltaic system using robust parametric methods. *IET Power Electron.* **2020**, *13*, 3661–3674. [CrossRef]
8. Zheng, W.; Xiong, X. Model identification method for photovoltaic grid-connected inverter based on Wiener model. *Proc. CSEE* **2013**, *33*, 18–26. [CrossRef]
9. Phan-Tan, C.-T.; Hill, M. Efficient Unbalanced Three-Phase Network Modelling for Optimal PV Inverter Control. *Energies* **2020**, *13*, 3011. [CrossRef]
10. Zhu, G.; Ruan, X.; Wang, X.; Yang, Z. The suppression of secondary ripple current and the improvement of dynamic characteristics of two-stage single-phase inverter. *Proc. CSEE* **2013**, *33*, 72–80, 188. [CrossRef]
11. Wang, J.; Lu, X.; Zhang, F.; Gong, C. Low-frequency ripple analysis and suppression of input current of two-stage single-phase inverter. *Proc. CSEE* **2012**, *32*, 10–11. [CrossRef]
12. Ma, K.; Huang, G.; Ma, L.; Zhang, X.; Wang, Z. Design of grid-connected inverter with adaptive reactive power and harmonic compensation function. *J. Power Supply* **2015**, *13*, 1–6. [CrossRef]
13. Liu, B.; He, J.; Su, M.; Sun, Y.; Wang, H.; Tang, Q. Two-stage single-phase inverter input ripple current double feedback suppression. *Trans. China Electrotech. Soc.* **2013**, *28*, 187–193, 217. [CrossRef]
14. Hailan, Z.; Longyun, K.; Xinwei, D.; Ming, Z. Secondary ripple suppression strategy for a single-phase PWM rectifier b-Zased on constant frequency current predictive control. *IEICE Trans. Electron.* **2022**. [CrossRef]
15. Tian, J. Research on Efficiency Optimization Methods for Two-Stage Inverters. Master's Thesis, East China Jiaotong University, Nanchang, China, 2017.
16. Yuan, Y.; Zhang, Y.; Zhong, Q.; Hu, G. Secondary ripple analysis and suppression of bus voltage of two-stage inverter. *J. Power Supply* **2018**, *16*, 37–45. [CrossRef]
17. Zhang, B.; Wang, Q.; Zhao, M. Analytical solution for output voltage ripple coefficient of BOOST converter. *Electr. Eng.* **2022**. [CrossRef]
18. Erik, G.; Marius, G.; Michael, S.; Daniel, W.; Wolfgang, W.; Sibylle, D.; Clemens, G.; Julia, K. The Impact of an Overlaid Ripple Current on Battery Aging: The Development of the SiCWell Dataset. *Batteries* **2022**, *8*, 11. [CrossRef]
19. Tao, L.; Cheng, J.; Wang, W.; Gong, J. Power quality comprehensive compensation device based on distributed photovoltaic inverter. *Electr. Meas. Instrum.* **2018**, *55*, 51–56, 77. [CrossRef]

20. Zeng, Z.; Zhao, R.; Yang, H.; Tang, H.; Jin, L.; Zhu, M.; Tang, S. Multi-functional grid-connected inverterand its application in microgrid power quality customization. *Power Syst. Technol.* **2012**, *36*, 58–67.
21. Liu, H.; Zhou, L. Multi-functional grid-connected inverter and its application in microgrid connected to distribution system. *Proc. CSEE* **2014**, *34*, 2649–2658. [CrossRef]
22. Sreekumar, P.; Khadkikar, V. Direct Control of the Inverter Impedance to Achieve Controllable Harmonic Sharing in the Islanded Microgrid. *IEEE Trans. Ind. Electron.* **2017**, *64*, 827–837. [CrossRef]
23. Ge, L.; Yuan, X.; Yang, Z. Control System Design of Shunt Active Power Filter Based on Active Disturbance Rejection and Repetitive Control Techniques. *Math. Probl. Eng.* **2014**, *2014*, 864989. [CrossRef]
24. Yang, Q.; Liu, D.; Wang, H.; Chen, X. Unified control system for photovoltaic grid-connected generation and power quality regulation. *Power Syst. Prot. Control.* **2015**, *43*, 69–74. [CrossRef]
25. Zhang, G.; Zhang, T.; Ding, M.; Su, J.; Wang, H. Unified control of photovoltaic grid-connected generation and active power filter. *Autom. Electr. Power Syst.* **2007**, *31*, 61–66. [CrossRef]
26. Wu, T.-F.; Nien, H.-S.; Hsieh, H.-M.; Shen, C.-L. PV power injection and active power filtering with amplitude-clamping and amplitude-scaling algorithms. *IEEE Trans. Ind. Appl.* **2007**, *43*, 731–741. [CrossRef]
27. Cai, J.; Sun, Y.; Huang, Y. Integrated control of photovoltaic grid-connected generation and reactive power compensation. *J. Jiangsu Univ. Nat. Sci. Ed.* **2014**, *35*, 324–328. [CrossRef]
28. Zhang, Z.B.; Liu, J.Z.; Mei, H.M. The reactive power compensation characteristics of two-stage three-phase photovoltaic grid-connected power generation system. *J. Electr. Technol.* **2011**, *26*, 242–246. [CrossRef]
29. Bolsi, P.C.; Prado, E.O.; Sartori, H.C.; Lenz, J.M.; Pinheiro, J.R. LCL Filter Parameter and Hardware Design Methodology for Minimum Volume Considering Capacitor Lifetimes. *Energies* **2022**, *15*, 4420. [CrossRef]
30. Lv, H. Research on Harmonic Current and Resonance Suppression Strategy of Single-Phase Grid-Connected Converter. Master's Thesis, Huazhong University of Science and Technology, Wuhan, China, 2021.
31. Xue, T. Resonance Mechanism Analysis and Control Strategy Research of LCL Grid-Connected Inverter. Master's Thesis, Chongqing University, Chongqing, China, 2020.